

# TPC in $\gamma$ -ray astronomy above pair-creation threshold

D. Bernard<sup>a</sup>

<sup>a</sup>LLR, Ecole Polytechnique, CNRS/IN2P3, 91128 Palaiseau, France

---

## Abstract

We examine the performance of a TPC as a  $\gamma$ -ray telescope above the pair-creation threshold. The contributions to the photon angular resolution are studied and their dependence on energy is obtained. The effective area per detector unit mass for such a thin detector is the conversion mass attenuation coefficient. The differential sensitivity for the detection of a point-like source is then derived. Finally, the measurement of track momentum from deflections due to multiple scattering is optimized.

These analytical results are exemplified numerically for a few sets of detector parameters. TPCs show an impressive improvement in sensitivity with respect to existing pair-creation-based telescopes in the [MeV - GeV] energy range, even with the modest detector parameters of this study. In addition, gas TPCs allow an improvement in angular resolution of about one order of magnitude.

*Keywords:* gamma rays, telescope, TPC, pair production, angular resolution, sensitivity

---

## 1. Introduction

High-energy astrophysics focuses on the study of complex objects such as active galactic nuclei (AGN), pulsars and gamma-ray bursts (GRB), the spectral energy distributions (SEDs) of which comprise contributions from a number of processes [1], including synchrotron emission, synchrotron self-Compton scattering (SSC), the inverse scattering of external thermal photons from the accretion disk (ESC), and  $\pi^0$  decays. These studies suffer from the existence of gaps in the sensitivity of the available instruments, such as that between the Compton-scattering-based telescopes, that are mostly sensitive below 1 MeV, and the pair-based telescopes, that are mostly sensitive above 100 MeV. Pair-based telescopes also suffer from a poor angular resolution at low energy, making the analysis of dense regions of the sky difficult.

In this paper we present a characterization of the use of a thin detector as an active target for cosmic  $\gamma$ -ray detection in the pair-conversion regime, with the aim of improving the angular resolution and the sensitivity at low energy. The past missions and the presently operated Fermi/LAT and AGILE use thick detectors for which the photon conversion probability is close to unity and the effective area  $A_{\text{eff}}$  is the product of the geometrical area of the detector  $A$  and of the reconstruction efficiency  $\epsilon_r$ :  $A_{\text{eff}} = A \times \epsilon_r$ . In a thin detector for which the conversion probability is small, the effective area becomes proportional to the pair conversion mass attenuation coefficient  $H$  and to the detector mass  $M$ ,  $A_{\text{eff}} = H \times M \times \epsilon_r$ . In a thick detector, the optimization of the aspect ratio height/surface is therefore critical, while for a thin detector it does not affect the effective area to first order. Note that in a thick detector, the various possible conversion processes are in competition with each other, and Compton scattering prior to- or in place of- pair conversion

would become a problem at the lowest energy if low  $Z$  material were considered, an effect strongly reduced for a thin detector. A sample of previous works on the use of gas detectors for the detection of cosmic  $\gamma$  rays above the pair-creation threshold, sometimes in relation with a Compton telescope, can be found in Refs. [2, 3, 4].

## 2. Test detector parameters

We use a time projection chamber (TPC) as a test model of a thin detector. A TPC is a chunk of homogeneous matter, located inside a (say) uniform electric field  $\vec{E}$  ([5], and a recent review [6]). Charged tracks crossing the TPC ionize atoms/molecules on their path, after which the ionization electrons drift to the anode plane where (in a gas TPC) they are amplified, and collected. The collecting plane can be segmented so as to provide two coordinates  $x, y$  of the location of the ionization. The third coordinate  $z$  is provided by the drift time  $t$ ,  $z = v_d \times t$ . The drift velocity  $v_d$  ranges from  $O(\text{mm}/\mu\text{s})$  at saturation for liquids and solids, to  $v_d = O(\text{cm}/\mu\text{s})$  for gases when used with an appropriate quencher, a multi-atomic molecule on which drifting electrons collide and are cooled down. The size of the electron “cloud” increases during the drift due to diffusion, which places a limit to the useable drift length. The typical value of the diffusion coefficient is  $O(100 - 200 \mu\text{m}/\sqrt{\text{cm}})$  for the three phases considered here.

Note that amplification of the signal is easily performed in a gas, but not in a liquid. The smallness of the collected signal  $\approx 4000 e^-/\text{mm}$  in liquid argon (lAr) and the limitation of the electrical power available in space for the digitization electronics would make precision tracking difficult. To alleviate this limitation, double-phase systems have been developed: the electrons are extracted from a liquid TPC into a gas in which they are amplified efficiently [7, 8]. But for a use in space, the instability of the gas/liquid interface would be a problem. A

---

*Email address:* denis.bernard at in2p3.fr (D. Bernard)

gas/solid system might be considered such as solid argon and a neon-based gas. The density and electron parameters of noble-gas solid and liquid are close enough that we neglect the difference and we use the liquid as representing the two dense phases<sup>1</sup>.

These analytical results are exemplified numerically for a few sets of detector parameters : three noble gases: neon, argon and xenon; three “densities”: gas at 1 and 10 bar, and liquid. We chose on purpose rather modest detector parameters, a detector mass  $M = 10$  kg and a tracking length of  $L = 30$  cm for gas,  $M = 100$  kg and  $L = 10$  cm for liquid, except in the case where the radiation length  $X_0$  would be shorter than  $L$ : in that case the propagation of an electron would be affected by radiation after a path length of the order of  $X_0$ , and we use  $L = X_0$ . The tracking length  $L$  is obviously related to the detector thickness, but they can be different, as in the case of liquid xenon. The sensitive mass for a gas TPC is chosen to be smaller due to the volume limitation of space missions.

We use typical values for the longitudinal sampling of the TPC,  $l = 1$  mm, and of the point space resolution,  $\sigma = 0.1$  mm.

### 3. Angular resolution

We consider a photon with energy  $E$  converting to an electron-positron pair in the field of a charged particle of the detector. The conversion is said to be “nuclear” in the case of an ion,  $\gamma Z \rightarrow e^+ e^- Z$ , and “triplet” in the case of an electron  $\gamma e^- \rightarrow e^+ e^- e^-$ . From momentum conservation:

$$\vec{p}_\gamma = \vec{p}_{e^+} + \vec{p}_{e^-} + \vec{q}, \quad (1)$$

we can identify several contributions to the photon angular resolution: (1) the single track angular resolution; (2) the fact that, in the case of nuclear conversion, the recoil momentum  $q$  of the ion, of the order of  $1 \text{ MeV}/c$  produces a path length that is too small to allow a measurement of  $q$ ; (3) the resolution of the norm of the momentum, named here the momentum resolution, for each of the hard tracks. We examine these three contributions in the following.

#### 3.1. Single track angular resolution

The basis of the understanding of tracking in the presence of multiple scattering was settled by Gluckstern [10]. We make use of the similar results derived by Innes for optimal fits [11]. We use an approximation of the multiple scattering angle  $\theta_0$  undergone by a particle of momentum  $p$  crossing a slab of matter with thickness  $x$  [12]:

$$\theta_0 = \frac{p_0}{\beta c p} \sqrt{\frac{x}{X_0}}, \quad (2)$$

where  $p_0 = 13.6 \text{ MeV}/c$  and we have neglected the negative logarithmic correction factor. At high momentum, multiple

scattering can be neglected and the detector resolution dominates [11] :

$$\sigma_{\theta tH} \approx \frac{8\sigma}{L} \sqrt{3/(N+5)}, \quad (3)$$

where  $N$  is the number of samplings,  $N = L/l$ . In the expressions of  $\sigma_\theta$ , the subscript  $t$  refers to a track and  $H$  and  $L$  to the high and low track momentum, respectively.  $\sigma_{\theta tH}$  is independent of the track momentum and improves like  $L^{-3/2}$  at given sampling  $l$ . On the contrary, multiple scattering dominates at low momentum; from the results of Ref. [11] and using the approximation of eq. (2), we obtain:

$$\sigma_{\theta tL} \approx (2\sigma)^{1/4} l^{1/8} X_0^{-3/8} (p/p_0)^{-3/4}. \quad (4)$$

The expression does not depend on the tracking length. This is because the end of the track contributes no information about the particle’s direction at the detector entrance once there has been sufficient scattering [11]. The  $p^{-3/4}$  dependence on momentum obtained here is comparable to the  $E^{-0.78}$  dependence on energy parametrized by the Fermi Collaboration [13]. The momentum limit between the two regimes is at  $p = p_{lim}$ , with:

$$p_{lim} = p_0 \times a_p \frac{L^2}{\sigma \sqrt{X_0 l}}, \quad (5)$$

where  $a_p = (2/8^4 \times 9)^{1/3} \approx 0.038$ .

#### 3.1.1. From tracks to photon

Combining the measurements of the directions of the electron and of the positron in the small-angle approximation, the direction of the reconstructed photon (with respect to the (unknown) true incoming direction) is  $\theta_\gamma = r\theta_{x+} + (1-r)\theta_{x-}$ , where  $r$  is the fraction of the energy that is carried away by the positron and  $\theta_{x+}$  and  $\theta_{x-}$  are the angles of the positron and of the electron, respectively. We then compute the photon angular resolution from the track angular resolution, eqs. (3),(4).

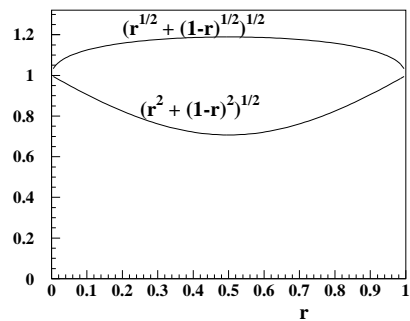


Figure 1: Track-to-photon angular resolution factors as a function of the fraction  $r$  of the photon energy carried away by the positron.

In the multiple scattering dominated regime we obtain  $\sigma_{\theta\gamma} = \sigma_{\theta t} \sqrt{\sqrt{r} + \sqrt{1-r}}$  and in the high energy regime:  $\sigma_{\theta\gamma} = \sigma_{\theta t} \sqrt{r^2 + (1-r)^2}$ , in the expressions of which the track momentum  $p$  is replaced by the photon energy  $E$ . The photon

<sup>1</sup>Note that liquid neon does not allow electron to drift, but solid neon does [9].

angular resolution is therefore obtained from the single track angular resolution by applying a correction factor that is close to unity (Fig. 1) and that we neglect in the following.

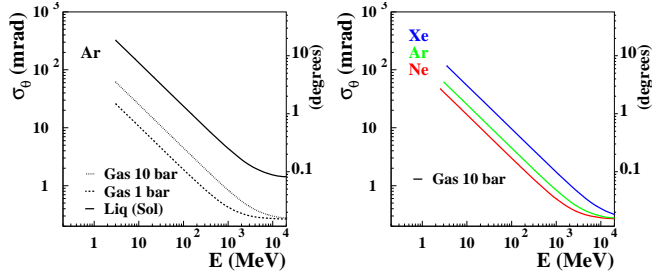


Figure 2: (Color online). Dependence of the RMS photon angular resolution on photon energy, in argon for various densities (left) and in 10 b gas for various gases (right).

Assuming a quadratic sum of  $\sigma_{\theta H}$  and of  $\sigma_{\theta L}$  in the intermediate energy range, we can examine the energy dependence of the photon angular resolution due to single track angular resolution (Fig. 2). Less dense TPCs have a better resolution. The difference in the high-energy asymptotic values, between gas and liquid, is due to the shorter tracking length used here, 10 cm vs 30 cm.

### 3.1.2. Recoiling ion

In the case of nuclear conversion, the recoil momentum goes undetected, unless a very low pressure TPC is used. The recoil is almost transverse to the photon direction, and the contribution to the photon angular resolution is therefore  $\approx q/E$ . The  $q$  distribution for nuclear conversion has been obtained by Jost et al. [14]<sup>(2)</sup> by the integration of the 5D Bethe-Heitler differential cross section [15]. It has a very wide spectrum that extends from  $2m^2/E$  to  $E$  at high energy, where  $m$  is the electron mass. The spectrum peaks at a value of the recoil momentum  $q_M$  that decreases with  $E$  (Fig. 3).

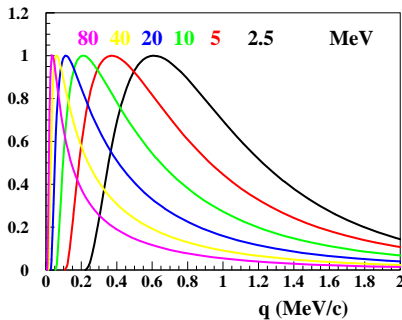


Figure 3: (Color online). Distribution of the recoil momentum for several incoming photon energies, from Ref. [14], in the approximation of no screening, normalized to unity at their maximum.

The 68 % containment value  $q_{68}$  of  $q$  is of particular interest as the point spread function of  $\gamma$  telescopes is often expressed in

<sup>2</sup>With Borsellino's correction [16] applied.

that way. The estimations of  $q_{68}$  from the 1D  $q$  distribution [14] and from the 5D Bethe-Heitler differential cross section [15] are found to be compatible with each other which constitutes a cross check (Fig. 4). Also of interest is the momentum at half-maximum  $q_{1/2}$ , on the decreasing slope above the maximum.

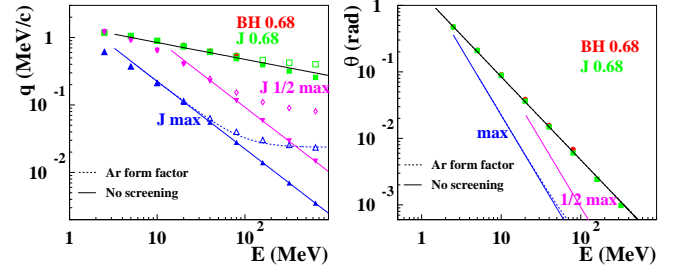


Figure 4: (Color online). Left: 68 % “containment” value  $q_{68}$  of the recoil momentum  $q$ , as a function of incoming photon energy  $E$ . ‘J’ stands for the  $q$  distribution by Jost et al. (squares) [14], while ‘BH’ stands for the 5D Bethe-Heitler differential cross-section (bullets) [15]. Values  $q_M$  of  $q$  at maximum (up triangles) and at half maximum  $q_{1/2}$  (down triangles). The solid symbols corresponds to the absence of screening, and the open symbols to screening parametrized by the Mott form factor [17]. Right: 68 % “containment” space angle induced by the non-observation of the recoiling nucleus. The upper line corresponds to  $\theta = 1.5 \text{ rad}[E/1 \text{ MeV}]^{-5/4}$ , the lower lines to  $q_{1/2}/E$  and  $q_M/E$ .

Under the approximation of no screening of the field of the nucleus by the surrounding electrons, we find  $q_M$  and  $q_{1/2}$  to vary like  $\approx 2.24 \text{ MeV}/(cE)$  and  $\approx 9.28 \text{ MeV}/(cE)$ , respectively, while  $q_{68}$  has a much milder dependence on  $E$ , as  $q_{68} \approx (1.5 \text{ MeV}/c)E^{-1/4}$ . Therefore, at high energy, a low- $q$  core develops that is narrower with increasing  $E$ , but that contains a fraction of events which decreases with  $E$ .

		No screening (low energy)		Screening (high energy)	
		$q$	$\theta$	$q$	$\theta$
$q_{68}$	68 % containment	$\propto E^{-1/4}$	$\propto E^{-5/4}$	constant	$\propto 1/E$
$q_M$	at maximum	$\propto 1/E$	$\propto 1/E^2$	constant	$\propto 1/E$
$q_{1/2}$	at half max	$\propto 1/E$	$\propto 1/E^2$	constant	$\propto 1/E$

Table 1: Dependence on photon energy of  $q_{68}$ ,  $q_M$ , and  $q_{1/2}$  and related angular shifts from  $\theta \approx q/E$ .

The dependence of  $q_M$ ,  $q_{1/2}$  and  $q_{68}$  on photon energy are represented in Fig. 4, and tabulated in Table 1. Closed symbols refer to the absence of screening. The screening of the field of the nucleus by the surrounding electrons can be described by multiplying the  $q$  distribution [14] by  $(1 - F(q))^2$ , where  $F(q)$  is the Mott atomic form factor  $F(q) = \frac{1}{1+(q/q_0)^2}$ , with  $q_0 = 111Z^{-1/3} \times m$  [17]. When screening is taken into account, the 68% containment value saturates at high energy to a value that has a mild  $Z$  dependence, and that is close to  $0.4 \text{ MeV}/c$ , while the distribution maximum  $q_M$  saturates to a much smaller value close to  $2 \times q_0$ . The induced photon angle shift is obtained simply by  $\theta = q/E$  (Fig. 4 right).

### 3.2. Contribution of track momentum resolution

The contribution of the track momentum resolution  $\Delta p$  in the reconstruction of the photon momentum is estimated using a generator of the 5D Bethe-Heitler [15] differential cross section, to which a momentum spread assumed to be of 10 % is added.

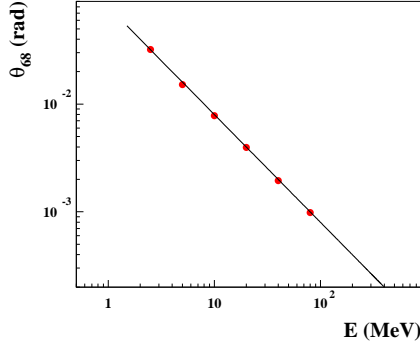


Figure 5: (Color online). 68% containment angle shift due to a track momentum resolution of  $\Delta p/p = 10\%$ , from a generation of the 5D Bethe-Heitler [15] differential cross section.

The dependence is found to be  $\theta \approx (\Delta p/p)0.8 \text{ rad}/E$  (Fig. 5). This  $1/E$  dependence was expected given the  $1/E$  dependence of the opening angle [18].

### 3.3. Angular resolution: a Summary

The results obtained so far are summarized in Fig. 6 (we have neglected the small difference between the RMS and the 68% containment values).

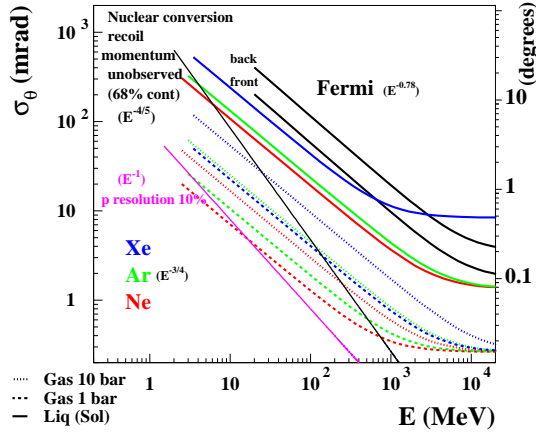


Figure 6: (Color online). Various contributions to the photon angular resolution.

- The single track angular resolution dominates;
- The missing momentum recoil contributes significantly at low energy, especially for low density TPC;
- The effect of a single track momentum resolution at a level of 10 % as assumed here is negligible.

A ten-fold improvement of the angular resolution with respect to the performance of the Fermi/LAT [13] is within reach with a gas TPC. A liquid xenon TPC shows a poor performance here, in contrast with its use as a Compton telescope[19].

## 4. Effective area

Assuming 100% reconstruction efficiency, which is reasonable for a TPC, we obtain the dependence on energy of  $A_{\text{eff}}$  (Fig. 7) from the tabulation of the mass attenuation coefficient in Ref. [20].

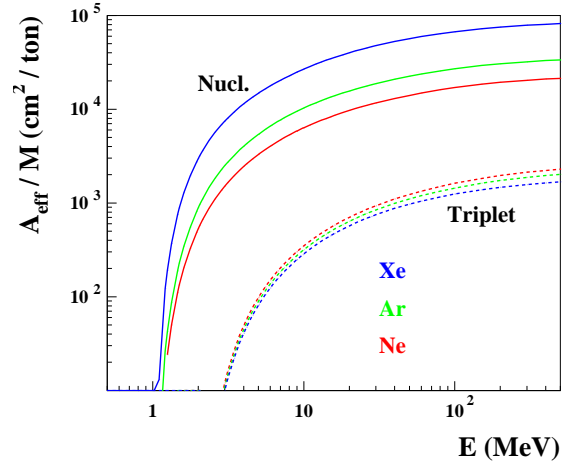


Figure 7: (Color online). Dependence on energy of the effective area per unit mass assuming 100% reconstruction efficiency [20].

In the case of triplet conversion, the effective area is almost independent of  $Z$  which is not surprising, as the number of electrons per unit mass is almost a constant of Nature.

## 5. Differential sensitivity

From the above we compute the sensitivity to the detection of a faint high-latitude point-like source. We mimic the computation of the Fermi/LAT sensitivity [13] with a simpler method.

We use four bins per energy decade ( $\Delta E = 10^{-1/4}E \approx 0.78E$ ), a  $n = 5$  standard deviation significance, a  $T = 3$  year observation time, an  $\eta = 17\%$  exposure fraction, and a minimum signal event number  $S \geq 10$ . The sensitivity is computed inside a  $\sigma_\theta$  68%-containment angle, and “against” the extragalactic  $\gamma$ -ray background [21]: we therefore compare our results to Fermi’s differential sensitivity at  $90^\circ$  galactic latitude [13].

### 5.1. Gaussian statistics

Using Gaussian statistics,  $n$  is simply obtained from the numbers  $S$  and  $B$  of signal and background events, respectively, from  $S = n\sqrt{B}$ . We compute these numbers of events as :

$$S = T \times \eta \times A_{\text{eff}}(E) \times I_0(E) \times \epsilon \times \Delta E \quad (6)$$

$$B = T \times \eta \times A_{\text{eff}}(E) \times \pi \sigma_{\theta}^2 \int F_B(E) dE \quad (7)$$

where  $F_B$  is the background flux,  $I_0$  the signal intensity, and  $\epsilon = 0.68$ , the efficiency of the angle cut. The sensitivity  $s$  expressed as the minimum detectable signal intensity, multiplied by  $E^2$ , that is  $s = E^2 \times I_0$ , is therefore:

$$s = E^2 \times I_0 = \frac{n \times E^2}{\epsilon \Delta E} \sqrt{\frac{\pi \sigma_{\theta}^2 \int F_B(E) dE}{T \times \eta \times A_{\text{eff}}}} \quad (8)$$

The factors that depend on  $Z$  are  $\sigma_{\theta} \propto X_0^{-3/8}$  and  $A_{\text{eff}} \propto H$  that is, asymptotically,  $A_{\text{eff}} \propto 1/X_0$ . These dependences cancel partially in the expression of  $s \propto \sigma_{\theta} / \sqrt{A_{\text{eff}}}$ , so that  $s \propto X_0^{1/8}$ : the  $Z$  dependence of the sensitivity as described by eq. (8) is extremely small.

## 5.2. Poisson statistics

Using Poisson statistics, and following the method used by Ref. [22] (A recent derivation of eq. (9) can be found in Ref. [23] eq. (96)), the significance  $n$  becomes such that:

$$n^2 = 2B[(1 + S/B) \ln(1 + S/B) - S/B], \quad (9)$$

which reduces to  $n^2 = S^2/B$  in the background-dominated regime  $S/B \ll 1$ , as expected. We solve eq. (9) for  $S$ , with  $n = 5$ .

Figure 8 shows the dependence on energy of the differential sensitivity for the nine test cases of this study compared to that of the Fermi/LAT [13] and of the Compton telescope COMPTEL [24]. On the left plot, an ideal case for which the missing recoil momentum could be neglected in the expression of the angular resolution, we see that a gas TPC would clearly have a better performance than a liquid TPC: the better angular resolution would outweigh the smaller sensitive mass (10 kg compared to 100 kg). In reality, the effect of the missing recoil momentum on the sensitivity is visible at low energy (right plot).

Together with Compton telescope projects, which aim at sensitivities of the order of  $10^{-5} \text{MeV}/(\text{cm}^2 \text{s})$  close to 1 MeV [25], there is good hope to fill the sensitivity gap between the energy ranges of the Compton and pair telescopes, and even to envisage enough overlap for a cross-calibration.

## 6. Track momentum from multiple measurement of multiple scattering

In this section we examine the potential of a TPC to determine the momentum of the conversion electrons from the deflection due to multiple scattering: since the average deflection angle  $\theta_0$  is proportional to  $1/p$ , each deflection provides a momentum measurement [26]. Bolton describes the relative momentum resolution  $\sigma_p/p$  as asymptotes of a ‘‘universal function’’ [27]:

- In the multiple scattering dominated regime (low momentum):  $\frac{\sigma_p}{p} = \frac{1}{\sqrt{2N}}$ , where  $N$  is the number of samplings.

- In the spatial resolution dominated regime (high momentum):  $\frac{\sigma_p}{p} = \frac{1}{\sqrt{2N}} \left( \frac{p}{p_m} \right)^2$ , where  $p_m = \frac{p_0 \Delta^{3/2}}{\sigma \sqrt{X_0}}$ , and  $\Delta$  is the length over which the deflection is measured, which must be larger than the sampling of the TPC,  $\Delta > l$ .

Approximating the full expression by the sum of the two asymptotes, we obtain:

$$\frac{\sigma_p}{p} = \frac{1}{\sqrt{2L}} \left[ \Delta^{1/2} + \frac{p^2 \sigma^2 X_0}{\Delta^{5/2} p_0^2} \right], \quad (10)$$

the minimum of which is obtained for:

$$\Delta = \left[ \frac{5p^2 \sigma^2 X_0}{p_0^2} \right]^{1/3}. \quad (11)$$

As the momentum is not known a priori, some iteration will be needed. The value of  $\sigma_p/p$  for that optimal set is:

$$\frac{\sigma_p}{p} = \frac{C}{\sqrt{2L}} \left[ \frac{p}{p_0} \right]^{1/3} \left[ \sigma^2 X_0 \right]^{1/6} \quad (12)$$

and  $C \equiv 5^{1/6} + 5^{-5/6} \approx 1.57$ . The method is usable at low energy, below 100 MeV (Fig. 9.)

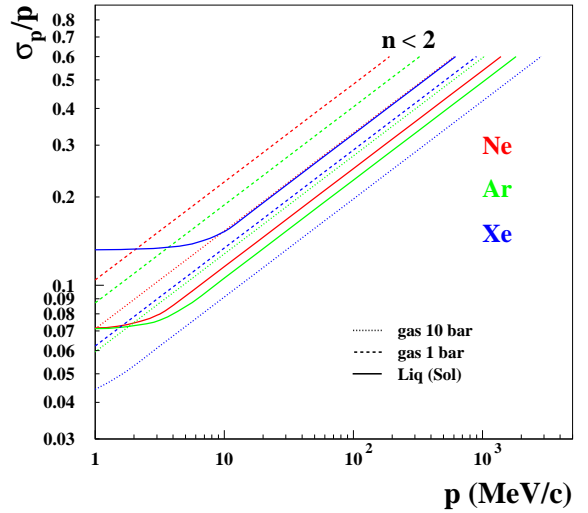


Figure 9: (Color online). Relative track momentum resolution for optimal sampling  $\Delta$  as a function of track momentum. (The low momentum asymptote for the liquids is due to the  $\Delta > l$  limit).

## 7. Summary

We examined the performance of a TPC as a  $\gamma$ -ray telescope above the pair-creation threshold. Analytical expressions are obtained for the various contributions to the photon angular resolution and the track momentum resolution. These analytical results are exemplified numerically. Even with the modest value of the parameters used in the present study, a  $L = 30 \text{ cm}$  tracking length and  $M = 10 \text{ kg}$  sensitive mass for gases and

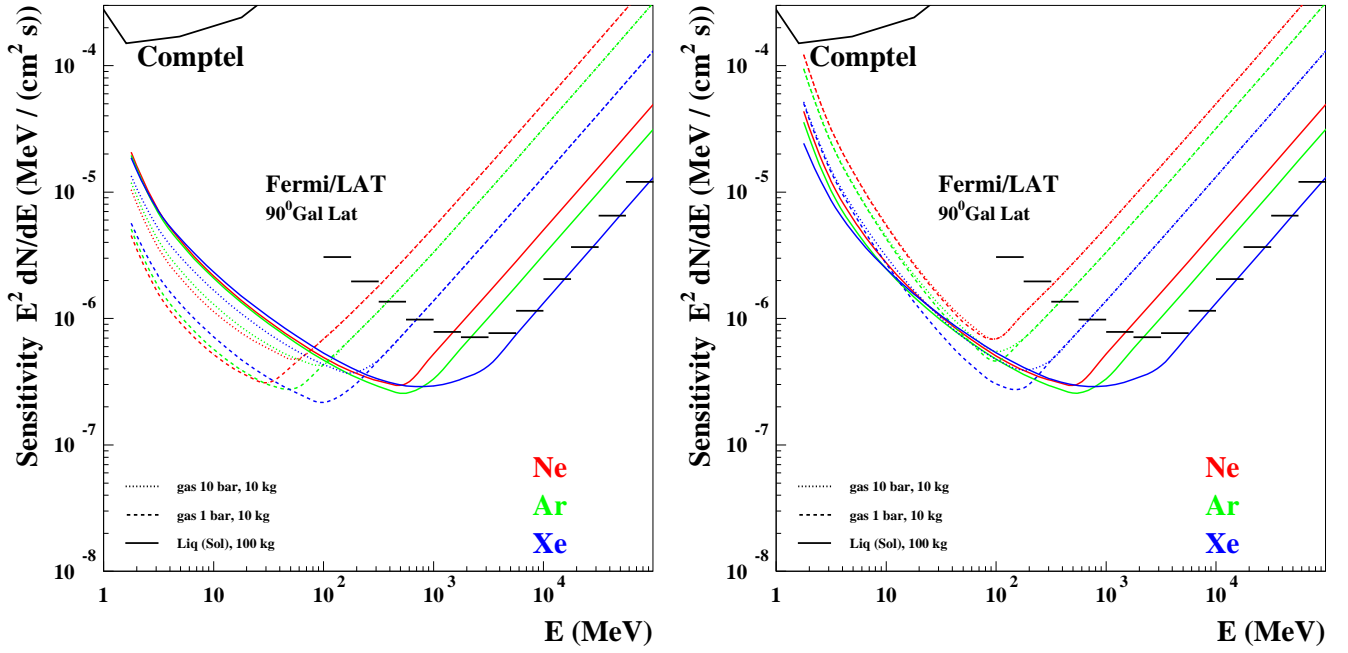


Figure 8: (Color online). Dependence of the differential sensitivity on photon energy compared to the  $90^\circ$  galactic latitude performance of the Fermi/LAT [13] and of the Compton telescope COMPTTEL [24]. Left : the ideal case in which the missing recoil momentum would be neglected in the expression of  $\sigma_\theta$ . Right : the real case, with the full expression of  $\sigma_\theta$ .

$L = 10$  cm tracking length and  $M = 100$  kg for liquids, TPCs show huge potential in the MeV-GeV range.

The angular resolution is found to have an  $E^{-3/4}$  energy dependence in the multiple scattering dominated energy range, except for gas TPC at low energy, where the missing recoil momentum dominates with a steeper dependence close to  $E^{-5/4}$ . An improvement of a factor better than ten in angular resolution with respect to the present tungsten-slab-converter telescopes is within reach for a gas TPC. This provides at least two orders of magnitude in background rejection, not to mention the easy albedo rejection and the immunity to cosmic-ray pile-up thanks to the detailed imaging provided by a TPC. The improved angular resolution translates also into a dramatic improvement of the differential sensitivity that will bridge up with a future Compton mission at a couple of MeV at a level of about  $10^{-5}$  MeV/(cm<sup>2</sup>s).

Track momentum can be measured from the deflections due to multiple scattering across the detector. After optimization of the sampling size, the momentum relative precision is found to vary like  $p^{1/3}$ . The method can be used for momenta smaller than  $100$  MeV/ $c$ . Above that limit, the photon energy measurement must be performed by an additional device. A TPC might well be a first layer of an otherwise high-energy (0.1 GeV - 3 TeV) range project such as Gamma-400 [28].

An R&D program is in progress to characterize the use of a TPC as a  $\gamma$ -ray telescope and as a  $\gamma$ -ray polarimeter [29, 30].

A number of approximations have been made in this work so as to obtain scaling laws in the form of analytical expressions that are easily handled. To name a few, we have neglected the logarithmic correction of multiple scattering, the loss of energy

of the tracks inside the detector, their emission of radiation that disturbs tracking at high momentum, especially for high-Z detectors and/or dense TPC – such as liquid xenon, and trigger inefficiency. These limitations would be addressed using a full simulation, which is beyond the scope of the present study.

## References

- [1] G. Ghisellini, “Radiative Processes in High Energy Astrophysics,” arXiv:1202.5949 [astro-ph.HE].
- [2] Hartman, R. C., “Astronomical gamma ray telescopes in the pair production regime”, Nucl Physics B Proc. Suppl., 10 (1989) 130.
- [3] Hunter, S. D.; Bertsch, D. L.; Deines-Jones, P. “Design of a Next Generation High-Energy Gamma-ray telescope”, GAMMA 2001: Gamma-Ray Astrophysics 2001. AIP Conference Proceedings, 587, 848-852 (2001).
- [4] K. Ueno *et al.*, “Development of the tracking Compton/pair-creation camera based on a gaseous TPC and a scintillation camera”, Nucl. Instrum. Meth. A **628**, 158 (2011).
- [5] D.R. Nygren and J. N. Marx, “The Time Projection Chamber”, Physics Today 31 (1978) 46.
- [6] D. Attie, “TPC review,” Nucl. Instrum. Meth. A **598**, 89 (2009).
- [7] A. Bondar “Two-phase argon and xenon avalanche detectors based on gas electron multipliers,” Nucl. Instrum. Meth. A **556**, 273 (2006).
- [8] A. Badertscher *et al.*, “First operation of a double phase LAr Large Electron Multiplier Time Projection Chamber with a two-dimensional projective readout anode,” Nucl. Instrum. Meth. A **641** (2011) 48.
- [9] V. Brisson *et al.*, “Performance Of A Prototype Solid Neon And Solid Argon Calorimeter,” Nucl. Instrum. Meth. **215**, 79 (1983).
- [10] R. L. Gluckstern, “Uncertainties in track momentum and direction, due to multiple scattering and measurement errors,” Nucl. Instrum. Meth. **24**, 381 (1963).
- [11] W. R. Innes, “Some formulas for estimating tracking errors,” Nucl. Instrum. Meth. A **329**, 238 (1993).
- [12] J. Beringer *et al.*, (Particle Data Group), Phys. Rev. D86, 010001 (2012).

- [13] “The Fermi Large Area Telescope On Orbit: Event Classification, Instrument Response Functions, and Calibration”, Fermi-LAT Collaboration, arXiv:1206.1896
- [14] R. Jost, J. M. Luttinger and M. Slotnick, “Distribution of Recoil Nucleus in Pair Production by Photons,” *Phys. Rev.* **80**, 189 (1950).
- [15] “The quantum theory of radiation”, W. Heitler, 1954.
- [16] “Momentum Transfer and Angle of Divergence of Pairs Produced by Photons”, A. Borsellino, *Phys. Rev.* **89**, 1023 - 1025 (1953).
- [17] N.F. Mott, H.S.W. Massey, “The Theory of Atomic Collisions”, University Press, Oxford, 1934.
- [18] H. Olsen, “Opening Angles of Electron-Positron Pairs,” *Phys. Rev.* **131**, 406 (1963).
- [19] E. Aprile *et al.*, “Compton Imaging of MeV Gamma-Rays with the Liquid Xenon Gamma-Ray Imaging Telescope (LXeGRIT),” *Nucl. Instrum. Meth. A* **593**, 414 (2008) [arXiv:0805.0290 [physics.ins-det]].
- [20] NIST, National Institute of Standards and Technology, Physical Reference Data, <http://physics.nist.gov/PhysRefData/>
- [21] A. A. Abdo *et al.* [Fermi-LAT Collaboration], “The Spectrum of the Isotropic Diffuse Gamma-Ray Emission Derived From First-Year Fermi Large Area Telescope Data,” *Phys. Rev. Lett.* **104**, 101101 (2010) [arXiv:1002.3603 [astro-ph.HE]].
- [22] A. A. Abdo *et al.* [Fermi-LAT Collaboration], “Fermi Large Area Telescope First Source Catalog,” *Astrophys. J. Suppl.* **188**, 405 (2010) [arXiv:1002.2280 [astro-ph.HE]].
- [23] G. Cowan, K. Cranmer, E. Gross and O. Vitells, “Asymptotic formulae for likelihood-based tests of new physics,” *Eur. Phys. J. C* **71**, 1554 (2011).
- [24] “Lessons learnt from COMPTEL for future telescopes”, Volker Schnfelder, *New Astronomy Reviews*, **48** 2004 193.
- [25] R. Diehl, “GRIPS and the Perspective of Next-generation Gamma-ray Surveys,” *PoS INTEGRAL* **2010**, 035 (2010) [arXiv:1107.4892 [astro-ph.IM]].
- [26] K. Pinkau, “Analysis procedure of gamma ray astronomy spark chamber data,” *Nucl. Instrum. Meth.* **104**, 517 (1972).
- [27] T. Bolton, “High-energy muon momentum estimation from multiple Coulomb scattering in dense detectors,” hep-ex/9705007.
- [28] A. M. Galper *et al.*, “Status of the GAMMA-400 Project,” arXiv:1201.2490 [astro-ph.IM].
- [29] D. Bernard and A. Delbart, “High-angular-precision gamma-ray astronomy and polarimetry,” *Nucl. Instrum. Meth. A* **695**, 71 (2012).
- [30] D. Bernard, “HARPO - A Gaseous TPC for High Angular Resolution Gamma-Ray Astronomy and Polarimetry from the MeV to the TeV,” *Nucl. Instrum. Meth. A*, In Press, arXiv:1210.4399 [astro-ph.IM].